ACS APPLIED MATERIALS & INTERFACES

Article

Surface Energy and Work Function Control of AlOx/ Al Surfaces by Fluorinated Benzylphosphonic Acids

Ffion Abraham, William E. Ford, Frank Scholz, Gabriele Nelles, Graham Sandford, and Florian von Wrochem

ACS Appl. Mater. Interfaces, **Just Accepted Manuscript** • DOI: 10.1021/acsami.6b02012 • Publication Date (Web): 19 Apr 2016

Just Accepted

ACS Publications

ACS Applied Materials & Interfaces is published by the American Chemical Society.
1155 Sixteenth Street N.W., Washington, DC 20036

Surface Energy and Work Function Control of AlO_x/Al Surfaces by Fluorinated Benzylphosphonic Acids

Ffion Abraham,[§] William E. Ford, Frank Scholz, Gabriele Nelles, Graham Sandford,[§] Florian von Wrochem**

Sony Deutschland GmbH, Materials Science Laboratory, Hedelfinger Strasse 61, 70327 Stuttgart, Germany.

[§]Department of Chemistry, Durham University, South Road, Durham, DH1 3LE, UK.

AUTHOR EMAIL ADDRESS.

Graham.Sandford@durham.ac.uk; Florian.vonwrochem@eu.sony.com

Abstract: The performance of organic electronic devices can be significantly improved by modifying metal electrodes with organic monolayers, which alter the physical and chemical nature of the interface between conductor and semiconductor. In this paper we examine a series of twelve phosphonic acid compounds deposited on the native oxide layer of aluminum (AlO_x/Al), an electrode material with widespread applications in organic electronics. This series includes dodecylphosphonic acid as a reference and eleven benzylphosphonic acids, seven of which are fluorinated, including five newly synthesized derivatives. The monolayers are experimentally characterized by contact angle goniometry and by X-ray photoemission spectroscopy (XPS), and work function data obtained by low-intensity XPS are correlated with molecular dipoles obtained from DFT calculations. We find that monolayers are formed with molecular areas ranging from 17.7 to 42.9 $Å^2$/molecule, and, by the choice of appropriate terminal groups, the surface energy can be tuned from 23.5 mJ/m^2 to 70.5 mJ/m^2. Depending on the number and position of fluorine substituents on the aromatic rings, a variation in the work function of AlO_x/Al substrates over a range of 0.91 eV is achieved, and a renormalization procedure based on molecular density yields a surprising agreement of work function changes with interface dipoles as expected from Helmholtz' equation. The ability to adjust energetics and adhesion at organic semiconductor/AlO_x interfaces has immediate applications in devices such as OLEDs, OTFTs, organic solar cells, and printed organic circuits.

KEYWORDS. Phosphonic acid, Fluoroaromatic, Self-assembled monolayer, Aluminum electrodes, Work function, Surface energy, Charge injection, Organic electronics.

Introduction

Fluoroorganic molecules have already found many applications within electronic products, notably in liquid crystal display (LCD) devices, due to the high electronegativity of the fluorine atom capable of inducing a strong dipole on any organic system, and the strong C–F bond being stable under many operating conditions. These properties can be advantageously exploited in self-assembled monolayers (SAMs)[1,2] on electrode surfaces in organic electronic devices such as OLEDs[3] or OTFTs.[4]

A key electrode property that can be tuned using SAMs is the work function, because it is well known that a layer of electrical dipoles can substantially shift the electrostatic potential at the interface (surface potential), provided that the molecules in the layer possess a dipole moment component that is perpendicular to the surface.[5-7] In organic light emitting diodes (OLEDs), for example, where the efficiency strongly depends upon the height of the Schottky barriers at each of the respective electrode-semiconductor contacts, the insertion of a dipolar SAM between the electrode and the organic material allows the manipulation of the energy barrier through the interface and provides a significant degree of control over the electrical characteristics of the system.[5,8,9] Thus, to maximize the impact of molecular dipoles on the work function of the modified surface, a dense molecular packing and the alignment of the molecular dipoles along the substrate normal is highly desirable.

Besides tuning the electronic behavior of interfaces where two materials interact, the insertion of a SAM also provides a means to engineer the adhesion strength between the substrate and the subsequently deposited layers.[10] Bare metal oxide electrodes often possess high surface free energies due to the presence of hydroxyl groups, which significantly increase the hydrophilicity of the electrodes. From a device perspective, high surface free energies are often undesirable as subsequently deposited organic layers are characterized by a rather low surface energy. Such a mismatch is often responsible for poor wetting at the interface, leading to weak adhesion and eventually to device failure.[11,12] Depending on the terminal functional group that the SAM exposes to the surface, the surface energy can be substantially lowered,[13] thereby providing a more even

coverage, resulting in better device performance and long term stability.[9,11] Furthermore, the adhesion force between an electrode surface and an aromatic organic layer can be strengthened through the presence of π-π stacking interactions between the SAM and the organic semiconductor. By tuning the terminal functional group of the SAM to resemble functional groups present within the organic semiconductor, enhanced interactions at the interface may be achieved, which is the reason why SAMs in electronic devices often contain pendant aromatic substituents analogous to those of the deposited organic layer.[11,14]

In this paper, we aim for the modification of aluminum surfaces, because aluminum electrodes are among the most common and affordable electrode materials used in organic electronics, having applications in OLEDs, OTFTs, OPVs, and printed electronics. The native oxide layer on aluminum films (abbreviated AlO_x/Al) is decorated with phosphonic acid (PA) monolayers, a choice determined by the robustness of the PA anchor group on AlO_x, which has been advantageously exploited in organic thin-film transistors (OTFTs),[14-16] biocompatible materials,[17] and for corrosion resistance.[18] We demonstrate the versatility of highly dipolar fluorinated benzylphosphonic acids for tuning the work function of AlO_x/Al electrodes, as well as to adjust the surface free energy (or adhesion) of the substrate. To our knowledge, this is the first systematic study showing the dependence of the work function of alumina surfaces on the molecular dipole moment of the deposited adsorbates.

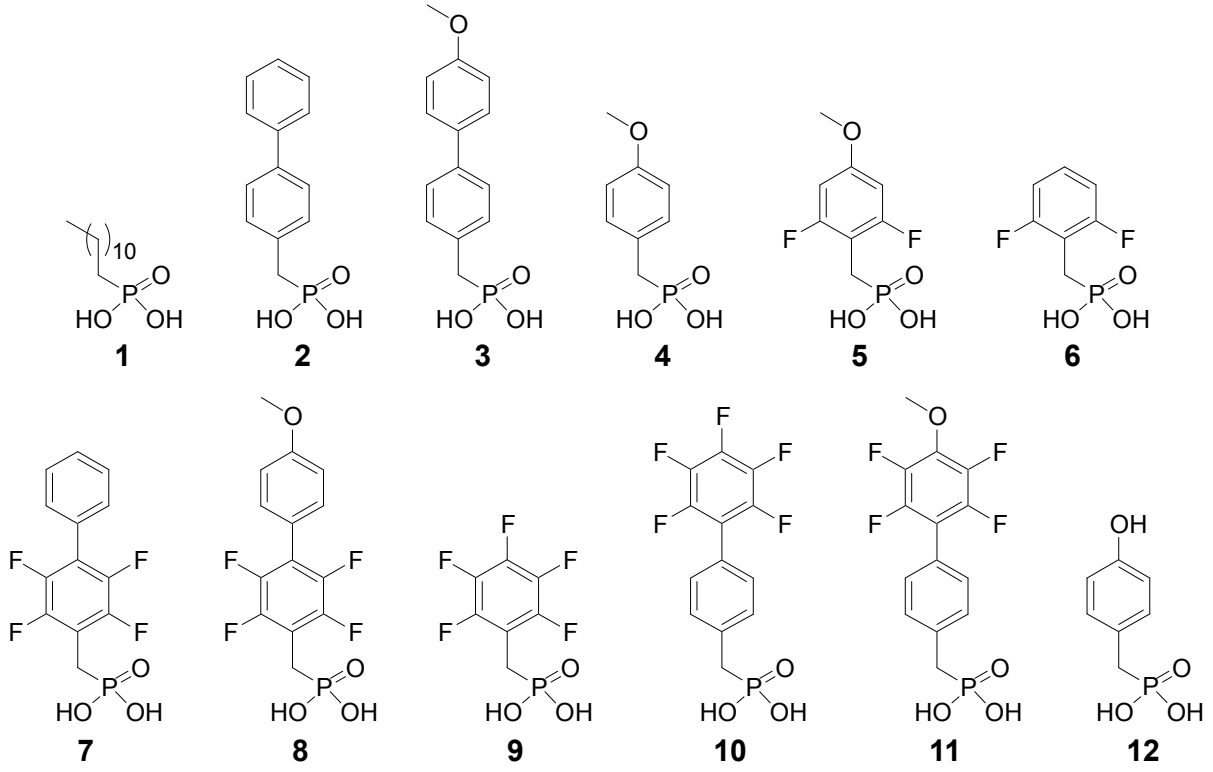

Figure 1. Chemical structures of the phosphonic acids **1 - 12** used in this study for the modification of AlO_x/Al surfaces.

Experimental Section

Materials. Absolute ethanol, the solvent used for self-assembly, was purchased from Merck KGaA, and diiodomethane (DIM), used for contact angle measurements, was purchased from Aldrich, all commercially bought solvents were used as received. Deionized water was from a Millipore system (18.2 MΩ·cm). Aluminum powder (0.2-0.7 mm, 99.9 %) was obtained from Thin Film Products. All PAs used were synthesized following the procedures described in the Supporting Information, with the exception of **1** and **12**, both of which were purchased from Epsilon Chimie and were used as received. Microscope cover glasses (10 mm × 10 mm or 10 mm × 20 mm) were purchased from Karl Hecht GmbH and were washed with distilled water and baked at 450 °C for 20 minutes just prior to use. Al films (110 nm) were deposited onto the glass slides by thermal evaporation (Univex 350, Leybold Vakuum GmbH). The Al films were subsequently stored under ambient conditions, whereupon an amorphous native oxide (AlO_x) layer develops spontaneously.[19,20]

Sample preparation: Pre-cleaning of the AlO_x/Al substrates. Prior to the deposition of monolayers of PAs on metal oxides, it is desirable to remove residual organic adsorbates, which can compete with the PAs for binding sites. During our initial investigations, we examined three methods of cleaning the AlO_x/Al substrates before depositing the SAMs: solvent cleaning (SC), solvent cleaning followed by UV-ozone treatment (SC/UVO), and solvent cleaning followed by oxygen plasma treatment (SC/OP). UV-ozone and oxygen plasma treatments remove organic sorbates through the generation of volatile oxygenated surface species that subsequently desorb. The SC procedure consisted of sonication of the AlO_x/Al/glass substrate in ethanol (4 minutes), followed by drying in a nitrogen flow. For SC/UVO cleaning, after the SC protocol, the substrate was treated in an UVO cleaner (Jelight Company, Inc., model 42-220) for 10 minutes, followed by immediate immersion into the PA solution. For SC/OP cleaning, following the SC protocol, treatment with oxygen plasma was performed in an O_2-fed plasma cleaner (GaLa Instrumente, model PlasmaPrep5) operated at 33 W for 4 minutes, again followed by immediate immersion into the PA solution. These three cleaning procedures were evaluated by contact angle measurements (see Supporting Information). If the surface has been adequately cleaned, its contact angle with water should approach 0°. On this basis, the SC/UVO and SC/OP methods both provided highly hydrophilic surfaces (contact angles with water ~10°). We decided to use the SC/UVO pretreatment as a standard protocol for all PAs, however, because it is less likely to alter the physicochemical nature of the oxide surface compared to the SC/OP method, thereby providing substrates that are more reproducible for SAM deposition. It is known that oxygen plasma can etch the AlO_x layer and oxidize the Al layer of AlO_x/Al substrates.[21] We also suspect that the plasma treatment, which is carried out in dry, low pressure conditions, may result in a loss of surface hydroxyl (OH) groups from the AlO_x layer. This is less likely to occur during the SC/UVO treatment, which is performed in the lab atmosphere. It is generally accepted that surface hydroxyl groups promote the adsorption of phosphonic acids onto metal oxides, including AlO_x/Al.[22] The thickness of the AlO_x layer on the SC/UVO-cleaned substrates was in the range 3.6 to 4.7 nm, as determined by XPS using a reported procedure.[23]

Monolayer formation. Self-assembled monolayers of PAs on AlO_x/Al were prepared under ambient conditions at room temperature as follows: after pre-cleaning, the substrates were fully immersed in a ~4 mM solution of the corresponding phosphonic acid in absolute ethanol for 18-26 h. The substrates were then rinsed copiously in ethanol to remove any unbound material, dried in a stream of nitrogen gas and either used immediately or stored under vacuum until required.

Contact angle goniometry. Static contact angle goniometry measurements were performed using a drop shape analyzer (DSA-30) from Krüss GmbH (Hamburg, Germany) with an automated drop dispenser and image video capture system. Immediately before data acquisition, the sample was rinsed with ethanol and dried in a nitrogen stream. Droplets of either water or diiodomethane (DIM) having volumes between 0.4 μL and 0.7 μL were deposited from a 0.5 mm diameter needle at different positions on each sample. Images were analyzed with the drop shape analysis software to determine the contact angle by circle fitting. Contact angle (θ) values reported (see **Table 1**) are averages of measurements of at least three drops for each solvent. The values of total surface energy (γ_S) and its dispersive (γ_S^D) and polar (γ_S^P) components were calculated from the contact angles with the method of Owens and Wendt[24] using software provided with the instrument.

X-ray photoemission spectroscopy. XP spectra were recorded using a Kratos Axis Ultra with a monochromated Al K_α emission source (1486.6 eV) operated at 15 kV and 180 W. The photoelectrons were collected in normal emission geometry by a hemispherical analyzer. An instrumental energy resolution of ~0.5 eV was achieved using a pass energy of 40 eV for the analyzer. The energy scale was referenced to the Au $4f_{7/2}$ line, located at a binding energy (BE) of 84.0 eV. For all samples, high resolution spectra of the C 1*s*, O 1*s*, F 1*s*, P 2*s*, and Al 2*p* regions, as well as survey scans, were acquired and deconvoluted using Gauss-Lorentz profiles (Voigt functions with 50:50 Lorentzian:Gaussian ratio) after subtraction of a linear background (Shirley background for Al 2*p*). To obtain elemental concentrations, XPS peak areas were normalized using instrumental relative sensitivity factors (RSF) calibrated with known reference samples. The molecular density of dodecylphosphonic acid monolayers, obtained from the P 2*s* signal intensity, was normalized with the aid of S 2*p* intensities from hexagonally close-packed 1-dodecanethiol ($C_{12}H_{25}SH$) reference

monolayers on template-stripped gold substrates. This was done by keeping both samples at equal heights in the measurement chamber. By comparison of the two intensities, the molecular density of 1-dodecylphosphonic acid monolayers was directly determined (using S 2*p* and P 2*s* RSF values of 0.668 and 0.344, respectively), and the remaining molecular densities for all other PAs extracted by means of P 2*s*/Al 2*p* ratios (using an RSF value for Al 2*p* of 0.294; see **Table 2**). Note that a similar hydrocarbon thickness can be assumed both for $C_{12}H_{25}SH$ and 1-dodecylphosphonic acid monolayers, as their coverage is very close (see Table 2). This can be deduced by the similar values of the RSF normalized intensity from P 2*s* and the S 2*p* signals, as well as by the fact that the C 1*s*/P 2*s* and C 1*s*/S 2*p* ratios for both SAMs are comparable. Thus, we could neglect attenuation factor differences for P 2*s* and the S 2*p* when comparing $C_{12}H_{25}SH$ and 1-dodecylphosphonic acid monolayers.

Overall, the error in the obtained molecular densities stems mainly from the limited P 2*s* signal intensity (statistical error of ~5% for the spectrometer settings used in our work), as well as from slight differences in the attenuation constant for P 2*s* and S 2*p* photoelectrons due to the dodecyl layer (systematic error of ~2-5%). The systematic error arising from the different substrate roughness (hence effective probed area) distinguishing template stripped Au (atomically flat) from AlO_x/Al (rough) can be neglected based on our AFM studies (<1%). However, a possible important systematic error stems from the RSF values for P 2*s* and S 2*p* core levels. This error can be minimized by RSF calibration using appropriate reference samples.

Binding energies were referenced to the hydrocarbon C 1*s* signal from the alkyl chains in SAM **1** at 285 eV, as this is common practice in the XPS literature[25] when no metallic emission signal (such as Au 4*f*) is available for calibration (note that the AlO_x layer forms an electrostatic dipole whose potential offset is thickness-dependent). For work function (Φ) determination at the low kinetic energy cutoff, low intensity XPS (LI-XPS) measurements were conducted. With a pass energy of 5 eV, an instrumental energy resolution of about 0.3 eV was obtained. The anode of the X-ray source was set to a voltage of 10 kV and the emission current adjusted to 1 mA to reduce the photon flux impinging the surface. As an energy reference, the Fermi level of a clean, argon ion-etched Au

surface was used (Φ = 5.12 eV), which is in agreement with reported values.[26] A bias voltage of -6 V was applied to the sample by means of a battery.

DFT calculations. Molecular dipole moments were determined by ground state density functional theory (DFT) calculations performed using the nonlocal generalized gradient approximation. These calculations were carried out at the PBE theory level[27] with a double numerical basis set including polarization functions (DNP) as implemented in the Dmol^3 program,[28] where an energy convergence of 10^{-6} Ha and 10^{-5} Ha has been employed during self-consistent field iterations and for structure relaxation, respectively. Dipole moment calculations were done by means of a coupled phosphonic acid/Al_6O_{10} cluster system, as illustrated in **Figure 2** for the pentafluorobenzyl-derivative **9**. We employed the Al_6O_{10} cluster as a simplified model of the AlO_x/Al surface, to which the phosphonic acid moiety was assumed to bind in the bidentate mode (see Ref.[29] for further discussion). This particular cluster, which is similar to cluster models investigated previously,[30-33] was the smallest one we could invent that provided two Al–OH groups in a geometry suitable for binding of the phosphonic acid moiety. Although the cluster itself is unrealistic with regards to the 3-fold coordination of Al atoms, we argue it is an appropriate model for the oxide layer found on aluminum, which can be described as non-crystalline and amorphous.[34,35] The projection of the dipole moment on the z-axis (μ_z, in units of Debye), defined as the axis perpendicular to the plane spanned by 4 Al atoms within the Al_6O_{10} cluster (marked with a dashed line in Figure 2), was computed for each PA-Al_6O_{10} system. The cluster was first relaxed using ethyl phosphonic acid as adsorbate. For the remaining series of PAs (**1**-**12**), the coordinates of the atoms within the Al_6O_{10} cluster (including the two bridging oxygen atoms bound to P) were kept fixed and only the organic residue (including P=O) was allowed to relax, hence preserving cluster geometry and binding configuration throughout the series. The simulation results for all PA-Al_6O_{10} cluster systems are available in the Supporting Information.

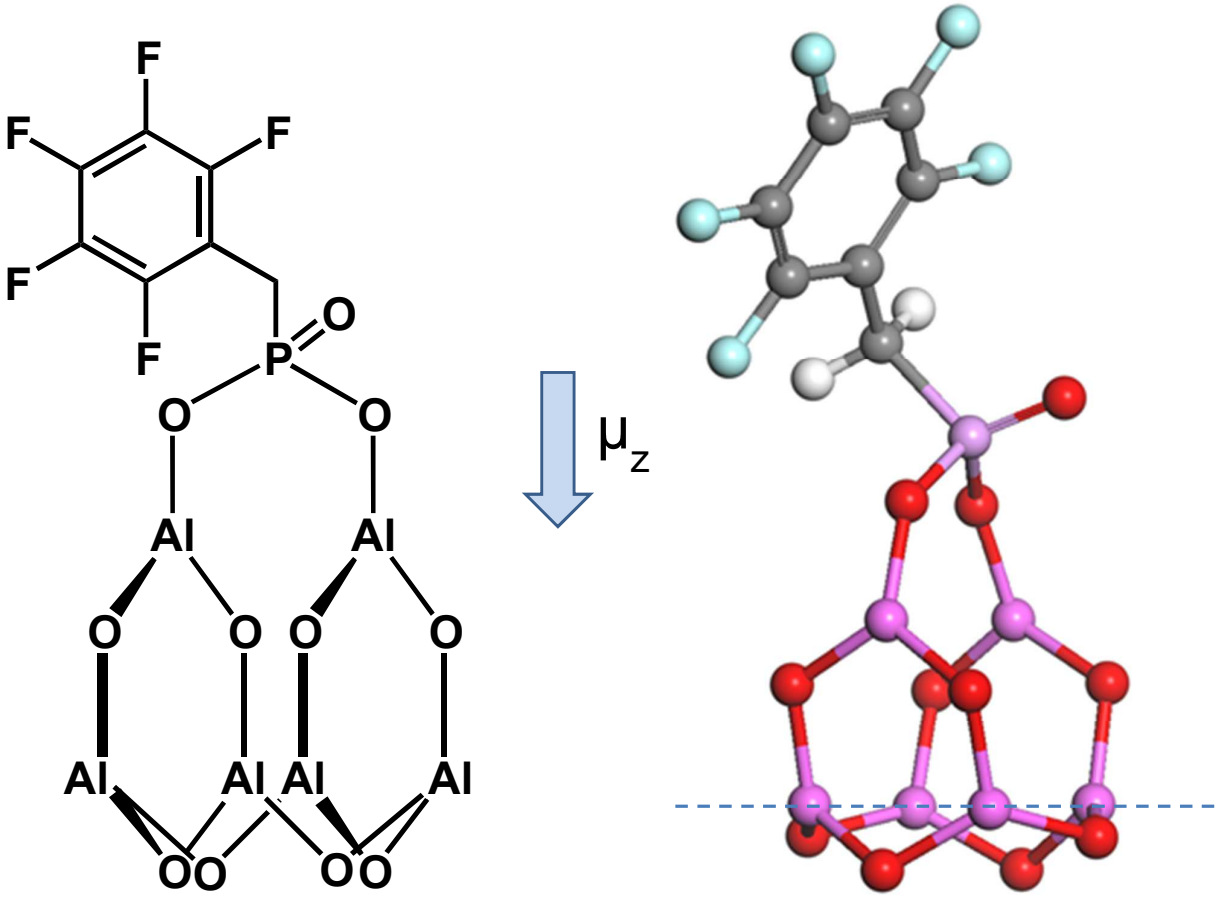

Figure 2. Coupled phosphonic acid–Al_6O_{10} cluster system as obtained from DFT calculations for determining the overall dipole moment, shown here with compound **9**. Both the molecular structure (left) and the ball and stick model (right) are shown. The arrow indicates the direction of the z-component of the dipole moment and the dashed line indicates the x-y plane defining the z-axis. The distance between the two O atoms linking the PA adsorbate to the Al_6O_{10} cluster is 2.57 Å (see Supporting Information).

Results

The phosphonic acids **1** to **12** used to prepare the monolayers on alumina are shown in Figure 1. These compounds were designed and selected to provide a possibly broad range of surface energies and work function values on AlO_x/Al electrodes. Five of the PA compounds (**5**, **7**, **8**, **10**, and **11**) are new and their syntheses provided in the Supporting Information. Of the remaining compounds, the adsorption of **9** on metal oxide surfaces has been the subject of numerous publications in recent years,[36-48] whereas **6** and **9** have been employed to modify the work function of crystalline ZnO surfaces.[36] For comparison, we have included dodecylphosphonic acid (**1**) in our study as a non-aromatic reference compound. Note that the phosphonic acid group that connects the fluoroaromatic backbone to the substrate excels in a strong bonding to metal oxides, producing layers of superior thermal and hydrolytic stability compared to other anchor groups (siloxane, carboxylic acid, etc.).[49-53] Thus, it represents an excellent platform for monolayer studies, as well as for applications that require a stable interface between electrode and organic semiconductor.

Contact angle goniometry. The surface free energy (γ_S) is a critical factor in determining the surface properties of solids such as wetting, adsorption, and adhesion. The ability to tune γ_S of metals or metal oxides by using self-assembled monolayers offers the possibility to improve adhesion between organic semiconductors and electrode structures in devices. Moreover, the modification of electrodes with SAMs results in surfaces having reproducible properties, unlike the case for bare electrodes, which are prone to marked variations in wettability or work function due to uncontrolled adsorption of atmospheric contaminants.

Although γ_S cannot be measured directly, several approaches exist for estimating it indirectly using semiempirical models with static contact angle goniometry.[54] In the Owens-Wendt method[24] used here, water (W) and diiodomethane (DIM) are used as probe liquids, and γ_S is approximated using the following three equations:

$$(\gamma_S^D \cdot \gamma_W^D)^{1/2} + (\gamma_S^P \cdot \gamma_W^P)^{1/2} = \gamma_W \cdot (1 + \cos\theta_W)/2 \quad (1)$$

$$(\gamma_S^D \cdot \gamma_{DIM}^D)^{1/2} + (\gamma_S^P \cdot \gamma_{DIM}^P)^{1/2} = \gamma_{DIM} \cdot (1 + \cos\theta_{DIM})/2 \quad (2)$$

$$\gamma_S = \gamma_S^D + \gamma_S^P \quad (3)$$

These equations are based on the assumption that the surface tension of the liquid phase (γ_W or γ_{DIM}) and the surface energy of the bare solid (γ_S) can be subdivided into dispersive (D) and polar (P) components. In this model, van der Waals interactions are dispersive and all other interactions (including dipole-dipole, π-π, and hydrogen bonds) are considered to be polar. The dispersive and polar components used for water are 21.8 mJ/m^2 and 51.0 mJ/m^2, respectively, and those for diiodomethane are 49.5 mJ/m^2 and 1.3 mJ/m^2, respectively.

The static contact angles and calculated surface energies of the SAMs (compared to a clean (SC/UVO) AlO_x/Al surface) are mainly given by the terminal group of the respective phosphonic acid compound, and are presented in Table 1 and **Figure 3**. The high surface energy (76.5 mJ/m^2) of the clean substrate reflects a high density of surface hydroxyl groups (Table 1). The contact angle values are highly reproducible, showing that well-defined surfaces are obtained by means of the present assembly procedure.

Table 1. Contact angles θ and surface energies γ_s of SAMs of phosphonic acids **1** to **12** on AlO_x/Al.

SAM	θ_W (°)	θ_{DIM} (°)	γ_S^D (mJ/m^2)	γ_S^P (mJ/m^2)	$\gamma_S = \gamma_S^D + \gamma_S^P$ (mJ/m^2)
1	109.3 ± 0.4	69.0 ± 0.8	23.4 ± 0.1	0.1 ± 0.0	23.5 ± 0.2
2	70.4 ± 1.3	33.9 ± 1.0	42.5 ± 0.2	6.5 ± 0.1	49.0 ± 0.3
3	68.0 ± 0.6	34.9 ± 0.8	42.1 ± 0.2	7.6 ± 0.1	49.7 ± 0.3
4	55.8 ± 1.5	33.9 ± 0.2	42.5 ± 0.0	13.7 ± 0.1	56.2 ± 0.2
5	67.5 ± 0.7	42.5 ± 0.5	38.3 ± 0.1	9.0 ± 0.1	47.3 ± 0.2
6	55.1 ± 1.0	45.0 ± 0.8	37.0 ± 0.2	16.3 ± 0.1	53.3 ± 0.3
7	75.5 ± 0.9	44.2 ± 1.9	37.4 ± 0.4	5.6 ± 0.1	43.1 ± 0.5
8	70.4 ± 1.2	35.0 ± 0.3	42.0 ± 0.1	6.6 ± 0.1	48.6 ± 0.1
9	81.1 ± 0.9	53.2 ± 0.9	32.5 ± 0.2	4.7 ± 0.1	37.1 ± 0.3
10	91.7 ± 0.3	58.3 ± 1.5	29.6 ± 0.3	1.9 ± 0.1	31.5 ± 0.3
11	82.9 ± 1.7	46.9 ± 0.5	36.0 ± 0.1	3.3 ± 0.1	39.2 ± 0.2
12	32.5 ± 2.3	26.1 ± 0.8	45.8 ± 0.2	24.7 ± 0.3	70.5 ± 0.5
SC/UVO[a]	11.6 ± 2.2	33.6 ± 1.6	42.7 ± 0.4	33.9 ± 0.4	76.5 ± 0.7

[a] Pre-cleaned substrate treated with absolute ethanol (no phosphonic acid).

As displayed in Figure 3, most of the PAs used in our study significantly decrease the overall surface energy of solvent/UVO cleaned AlO_x/Al substrates (from 76.5 mJ/m^2 down to 23.5 mJ/m^2). Mostly, the polar component (γ_s^p) is responsible for this reduction in surface energy.

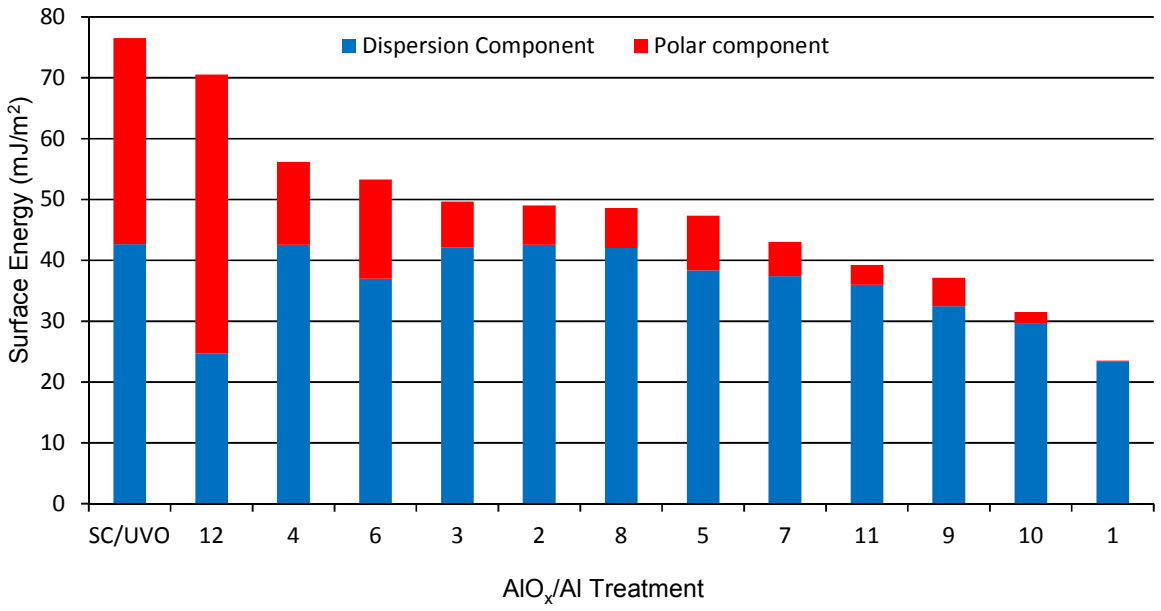

Figure 3. Surface energies comprising their polar and dispersion components for AlO_x/Al substrates after SC/UVO treatment and modification with phosphonic acids (see Figure 1 for the structures).

Several trends are evident when comparing surface energies and chemical substitution patterns (Figure 3). Apart from the monolayer of dodecylphosphonic acid (**1**), whose hydrophobic character results from close-packed alkyl chains exposing a high density of methyl groups to the surface, the lowest values of γ_S were obtained with the SAMs of pentafluorophenyl terminated PAs **9** and **10** due to the hydrophobic nature of the C–F bond.[55] Here, a minor difference in γ_S between **9** and **10** (~5.6 mJ/m^2) is attributed to different molecular densities (the denser SAM providing the more hydrophobic surface).

Of the five methoxy terminated SAMs, compounds **3**, **5** and **8** possess quite similar surface energies, whereas **4** and **11** show values >50 mJ/m^2 and <40 mJ/m^2, respectively. The increased surface energy observed for **4** is explained in terms of a higher molecular density compared to other methoxy-terminated SAMs. On the other hand, **11** is the only compound containing fluorine

substituents in *ortho* position relative to the methoxy substituent, and the close proximity of the fluorine atoms to the terminal functional group in this SAM, along with a large molecular tilt angle of the molecular backbone due to the bidentate bonding mode, can lead to a partial exposure of the *ortho* fluorine to the surface, hence to a reduced surface energy. The molecular orientation of (partially fluorinated) aromatic phosphonic acids has been studies by Gliboff *et al.*,[56] and revealed a tilt angle of 63° and 71° (angle between the ring normal and the surface normal) for non-fluorinated and fluorinated phenylphosphonic acid SAMs. For the present study on benzylphosphonic acid SAMs, mainly the molecular axis orientation is relevant, as it primarily affects the projected dipole moment component μ_z. This orientation is obtained by DFT calculations (see simulated molecular structures in the Supporting Information, with tilt angles in reasonable agreement with DFT results as reported in Ref[37]).

As far as the C–H terminated PAs **6**, **2**, and **7** are concerned, small differences in surface energy might originate from variations in coverage, fluorine substitution, or a combination of both factors. As expected, the highest surface energy (70.5 mJ/m^2) is obtained with the OH-terminated compound **12**, followed by the quite polar non-fluorinated methoxylated phosphonic acid **4**.

X-ray photoemission spectroscopy. As has been demonstrated in a broad range of monolayer studies,[2,57-59] XP spectroscopy is one of the most powerful methods for the chemical analysis of self-assembled monolayers. In the present study, we employed XPS (*i*) for the precise determination of surface coverage on AlO_x/Al substrates (as outlined below), and (*ii*) for the identification of the molecular species based on core level chemical shifts and heteroatom photoemission intensities. Representative results for a monolayer of **10** are shown in **Figure 4**.

Unlike the procedure used by Paniagua *et al.*,[48] who derived the coverage from contact angle data, and that used by Lange *et al.*,[36] who extracted the coverage from the dependence of the work function on molecular dipole moments, we determined the coverage of the phosphonic acid monolayers from XPS data. The basic procedure is illustrated in the following:

Method for molecular density determination by means of XPS data: As no reference phosphorous monolayer is available whose surface density is exactly known, the molecular densities of

dodecylphosphonic acid monolayers, obtained from XPS P 2*s* intensities, were normalized by means of S 2*p* intensities from close-packed dodecanethiol reference monolayers on gold substrates (note that hexagonally close packed dodecanethiol monolayers on Au have a well-known molecular area of 21.6 $Å^2$/molecule)[60]. For this purpose, absolute P 2*s* and S 2*p* intensities from dodecylphosphonic acid and dodecanethiol monolayers were acquired, making sure to keep both samples at equal heights in the analysis chamber of the spectrometer (i.e. keeping equal geometry during acquisition). Comparison of the two (RSF normalized) intensities yields the molecular density of dodecylphosphonic acid monolayers, with respect to close-packed alkanethiols (referred to as "coverage" in Table 2). The molecular density for all remaining PA monolayers (Table 2) was then extracted from the P 2*s*/Al 2*p* ratio for each sample, which is independent of photoelectron attenuation due to the molecular backbone since the P atom is located practically at the same distance from the AlO_x surface for all investigated SAMs. The P 2*s*/Al 2*p* ratio provides an absolute measure of the molecular density without any assumptions on surface roughness or depolarization parameters, as long as the energy of the X-ray source is much higher than the binding energy of the two relevant species, P 2*s* and Al 2*p*. Further details on the procedure used for density calibration, as well as an estimation of statistical and systematic errors, are reported in the experimental section.

Molecular densities and chemical analysis from XPS data. Overall, the monolayers presented in this study show medium to high densities on AlO_x/Al with molecular areas ranging from 17.7 $Å^2$/molecule for compound **6** (coverage = 1.22) to 42.9 $Å^2$/molecule for **9** (coverage = 0.50) (**Table 2**). The molecular area for **1** is close to that previously reported for monolayers of alkyl PAs on ZrO_2 (~25 $Å^2$).[61,62] Also included in Table 2 are values for the number of molecules per nm^2 (*N*, also referred to as the packing density), which is proportional to the coverage. In view of the molecular cross sections and the footprint of the PA group on AlO_x/Al substrates, or more specifically the question whether the PA group fits the substrate at the given densities, we can semi-quantitatively assess that the distance of the two oxygen atoms undergoing bidentate bonding to AlO_x/Al is 2.57 Å (see Fig. 2), which is smaller than the distance between the two sulfur atoms undergoing bidentate bonding to Au for dithiocarbamate SAMs (with an S-S distance of ~2.96 Å).[63] As dithiocarbamates

are known to assume packing densities comparable to those of dense alkanethiol SAMs,[9] also PA monolayers with similar densities should be possible (based on steric considerations only).

The rather broad distribution of densities found for the different PAs significantly affects the dependence of the work function on the molecular dipole moment, as detailed in the following section.

Table 2. Coverage, surface area per molecule, molecular density, work function, and molecular dipole moment of phosphonic acid SAMs on AlO_x/Al substrates.

SAM	Coverage[a]	Area (Å^2)[b]	N (nm^{-2})	Φ (eV)	Φ_{norm}[c] (eV)	μ_z[d] (D)	μ_z-μ_z^{ref} (D)
1	0.90_6	24.1	4.15	3.18	3.18	-2.664	0.000
2	1.22_9	17.7	5.64	3.57	3.47	-3.506	-0.842
3	0.73_0	29.6	3.38	3.62	3.72	-2.804	-0.140
4	0.91_7	23.8	4.20	3.41	3.41	-2.071	+0.592
5	0.56_3	38.4	2.61	3.55	3.77	-2.674	-0.010
6	0.77_7	28.2	3.55	3.27	3.29	-2.634	+0.030
7	0.51_5	42.8	2.34	3.50	3.75	-3.438	-0.774
8	0.77_1	28.0	3.57	3.58	3.64	-2.440	+0.224
9	0.50_3	42.9	2.33	4.08	4.78	-5.560	-2.896
10	0.74_2	29.1	3.43	4.09	4.28	-4.708	-2.044
11	0.67_2	32.1	3.11	3.71	3.89	-3.041	-0.377
12	0.97_6	22.4	4.47	3.82	3.77	-3.057	-0.393

[a]Coverage as determined from XPS data, relative to a SAM of $C_{12}H_{25}SH$ on Au(111). [b]Surface area per molecule, assuming a value of 21.6 Å^2/molecule for a reference SAM of $C_{12}H_{25}SH$ on Au.[60] [c]Work function from LI-XPS data, normalized for molecular density, N (see text). [d]Molecular dipole moment from DFT calculations of a coupled phosphonic acid/Al_6O_{10} cluster system.

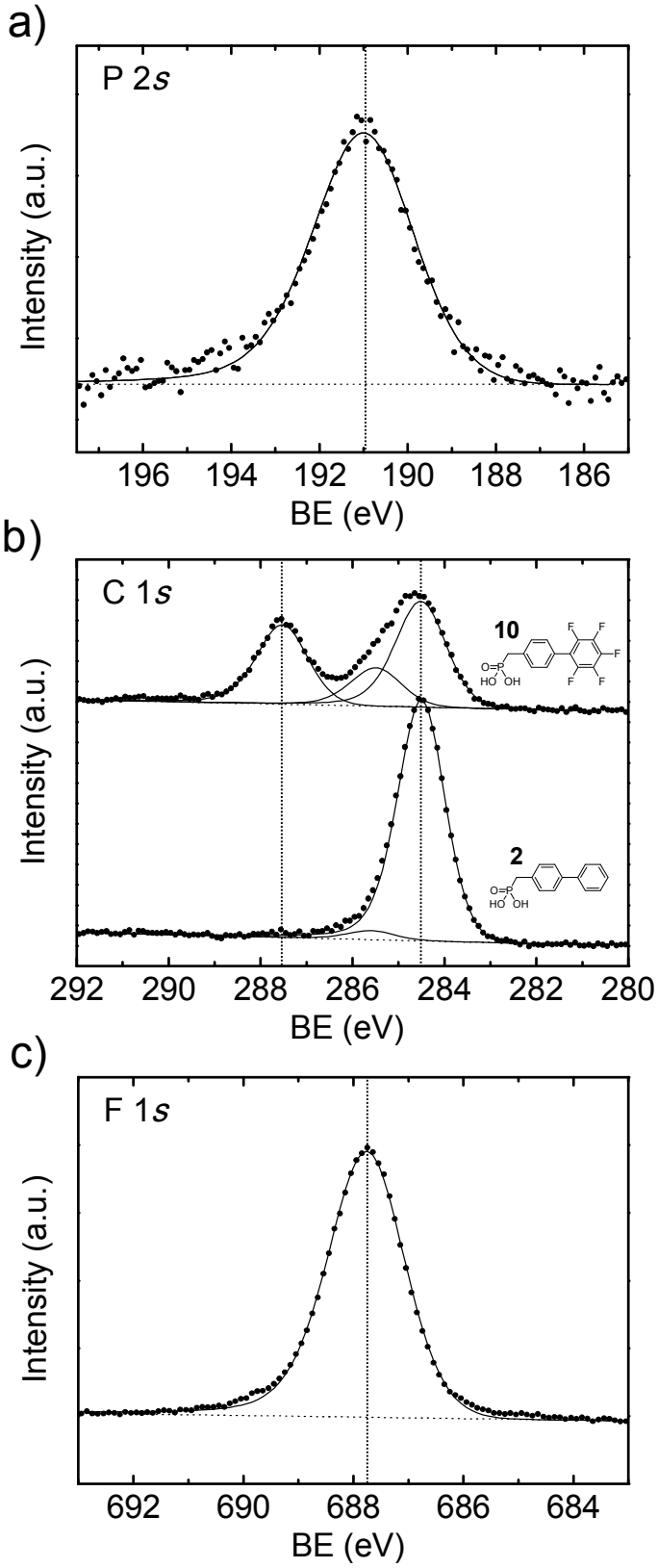

Figure 4. High resolution XPS spectra of phosphonic acid monolayers on AlO_x/Al. Data for compound **10** are shown here as representative spectra for all compounds. (a) P 2*s* core level at the energy of 191.0 eV. (b) C 1*s* signal, deconvoluted into 3 components according to the substitution pattern of the aromatic backbone. The species at 284.51 eV is assigned to aromatic carbon as confirmed by the analogous peak in the spectrum of compound **2**, only containing the biphenyl

moiety. The peak at 287.53 eV stems from fluorinated aromatic carbon. The component at 285.49 eV is assigned to carbon in the 1-position of the fluorinated ring (connected to the non-fluorinated phenyl), and also includes the methylene carbon. (c) F 1*s* signal with a single component at 687.76 eV, resulting from the fluorinated ring.

Whereas the O 1*s* signal from the phosphonic acid group cannot be resolved due to the strong AlO_x background from the substrate, P 2*s*, F 1*s*, and C 1*s* core levels show spectral characteristics and elemental areas that are in excellent quantitative agreement with molecular structure.[29] The chemical analysis of the phosphonic acid monolayers is accomplished by a careful study of the chemical shifts for the carbon C 1*s* signal, as shown in Figure 4b based on the representative compounds **2** and **10**. For **2**, a single C 1*s* species related to aromatic carbon (284.5 eV) is observed, whereas for **10** the C 1*s* signal is split among aromatic carbon (284.5 eV), fluorinated aromatic carbon (287.5 eV), and an intermediate species given both by the methylene carbon and by the carbon on the fluorinated ring that connects to the phenyl ring in *para*-position (285.5 eV). This intermediate component is broadened as it represents a superposition of two carbon species). The chemical shifts, related to the electronegativity of the substituents on the phenyl, are consistent with reported values and are discussed in detail in a second paper dedicated to spectroscopy.[29] It is anticipated that the analysis of the C 1*s* signal imposes an upper bound to the amount of unspecific contaminants adsorbed to the AlO_x/Al substrate, that within the accuracy of the XP method results to be <5% for most PA SAMs (except SAMs of **5** and **9**, showing higher amounts of unspecific hydrocarbons).

Work function modification. Tuning the work function (Φ) of electrodes by SAMs represents an important strategy to engineer organic electronic devices. Changes in the work function have been shown to correspond, at least qualitatively, to the Helmholtz equation:

$$\Phi_{SAM} = \Phi_0 + \Delta\Phi_{SAM} = \Phi_0 + \frac{e \cdot N \cdot \mu_z}{\varepsilon_0 \cdot \varepsilon_{SAM}} \qquad (4)$$

where Φ_0 is the work function of the "clean" surface, $\Delta\Phi_{SAM}$ the change in surface potential induced by the SAM, N is the density of molecules in the SAM, μ_z is the molecular dipole moment perpendicular to the surface, and ε_{SAM} is the dielectric constant of the SAM. The values of Φ for the

clean and SAM-modified AlO_x/Al samples are obtained by low-intensity XPS (LI-XPS) with sputtered gold (5.12 eV[9]) as an energy reference (see Supporting Information). The work function of the SC/UVO-cleaned AlO_x/Al is 3.84 eV, which is considerably higher than the value of 3.16 eV measured by Wang et al. under exclusion of atmosphere, representing the real work function of a pristine AlO_x/Al substrate.[64] However, the present value of Φ_0 (3.84 eV) falls within the typically reported range[65] and most likely reflects the adsorption of environmental contaminants during sample handling (note that the sample has to be transferred to the UHV chamber under ambient conditions). Fortunately, as indicated by the XPS results presented above, adsorbed contaminants are fully displaced by PAs during SAM formation, so that all changes in Φ can be directly related to molecular properties of the respective PA adsorbates. It is worth to mention that the work function of SAM **1** on AlO_x/Al (3.18 eV) is almost equal to that of pristine AlO_x/Al as reported by Wang et al., which we will make use of later on when normalizing Φ for variations in molecular density.

The values for μ_z are estimated from DFT calculations employing an Al_6O_{10} cluster to model the surface of AlO_x/Al. In this model, the phosphonic acid moiety is assumed to be bound in the bidentate mode (Figure 2; see Ref.[29] for further discussion), as this has already been reported to be the dominant binding mode in phosphonic acid monolayers by means of PM-IRRAS[48] and by comparative XPS and DFT studies[66] on ITO substrates. The PA-Al_6O_{10} model avoids artificial dipole contributions by the two P−OH groups of the free PA, which are strongly polar and whose directions are sensitive to the molecular structure. Also, it serves to define the z-axis to compute the dipole moment projection μ_z. Furthermore, although the effect of aromatic substitution on the electron density of the phosphonic acid group (for bidentate bonding) is reported to be small,[39] the coupled PA-Al_6O_{10} model takes into account possible charge reorganization at the PA-AlO_x/Al interface affecting the total interface dipole. Because the dipole of the Al_6O_{10} fragment deviates from the surface dipole of a realistic AlO_x/Al surface, we work with the difference $\Delta\mu_z = \mu_z - \mu_z^{ref}$ (Table 2). For μ_z^{ref} we use the (**1**)-Al_6O_{10} system because, as noted above, the work function Φ of SAM **1** on a AlO_x/Al surface is nearly the same as that of pristine AlO_x/Al (defined as Φ_0 in Eq. 4). Thus, $\Delta\mu_z$ represents the change in dipole moment upon deposition of a PA monolayer on AlO_x/Al.

The dependence of Φ on the computed dipole moment difference ($\mu_z - \mu_z^{ref}$) for PA SAMs **1**-**12** is shown in **Figure 5**a. Overall, the work function of the modified AlO_x/Al samples span a range of 0.91 eV, from 3.18 eV (**1**) to 4.09 eV (**10**) (Table 2). As indicated in the graph, the data points appear to fall into two groups: PAs terminated with OMe groups, and PAs terminated with either F- or H-atoms. The point for **12** was not included in any of the linear fits due to the unique nature of its terminal group (OH). Although both datasets indicate a roughly linear dependence of Φ on μ_z, Eq. 4 implies that linearity is given only when N and ε_{SAM} are constant. In the present case, however, N varies significantly within the SAM **1**-**12** dataset (see molecular density in Table 2).

We use Eq. 5 to normalize Φ for variations in N (see Supporting Information for a derivation of this equation) on the basis of molecular densities extracted from XPS data (see Results section):

$$\Phi_{norm} = \Phi_0 + \frac{N_{ref}}{N}(\Phi - \Phi_{ref}) \qquad (5)$$

Here, Φ_{ref} is the work function of the reference monolayer having the molecular density N_{ref}. Notably, Eq. 5 is only applicable if $\Phi_{ref} = \Phi_0$ (see Supporting Information) so we select SAM **1** as the reference because its work function (3.18 eV) is almost equal to that of pristine AlO_x/Al (3.16 eV).[64] The dependence of the normalized work function Φ_{norm} on the computed dipole moment is shown in **Figure 5b**. As in (a), the data points fall into two groups representing PAs with and without terminal methoxy substituents, where OMe-substituted PAs show a characteristic offset to higher work function values. This offset is exemplified by comparing PAs **5** and **6**: although their μ_z values differ by only 0.04 D, the work function with SAM **5** is 0.28 eV higher than with SAM **6**. The offset is even larger (0.48 eV) when one compares the normalized work functions. The source of this discrepancy is at present uncertain, and might be related to the interaction of the OMe-substituents with the molecular environment, not accounted for so far by DFT calculations. In fact, molecules terminated with polar methoxy groups may interact differently with their neighbors in the SAM than molecules terminated with less polar F- or H-atoms, which might result in a systematic work function shift.

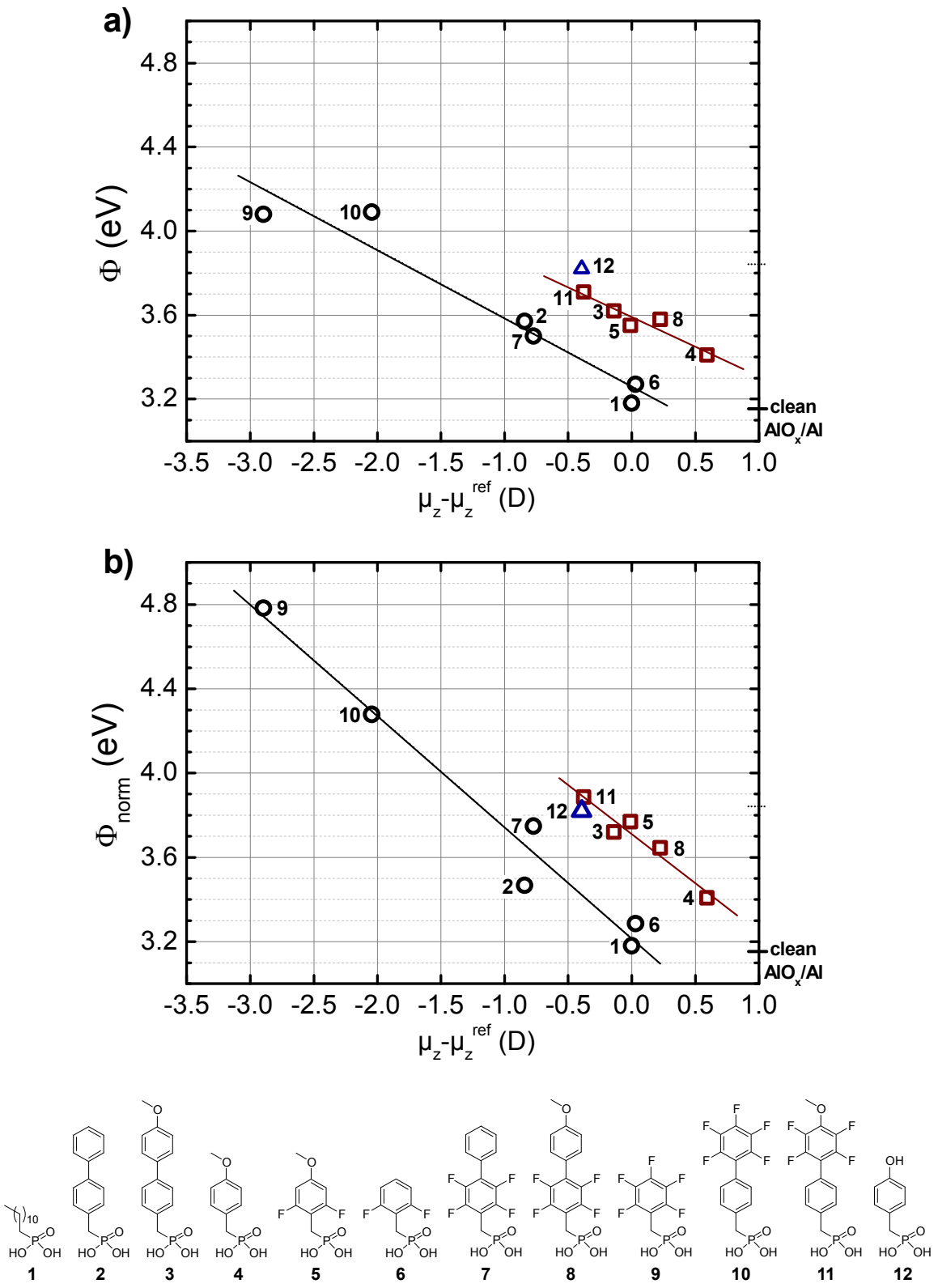

Figure 5. Dependence of the work function of AlO_x/Al on the molecular dipole moment of SAMs **1** to **12**. The circular and square points represent the PAs without and with methoxy-substituents, respectively; the triangular point is for SAM **12**. The dipole moments μ_z are computed for Al_6O_{10} cluster systems, as described in the experimental section. We use $\mu_z - \mu_z^{ref}$ as abscissa in these graphs, where μ_z^{ref} is the dipole moment for **1**-Al_6O_{10}. In graph (a) measured work function values are presented, whereas graph (b) shows normalized values (Φ_{norm}, see text); linear fits are indicated for the F/H-terminated and for the OMe-terminated PA compounds, separately. The value of Φ for clean

AlO_x/Al is from Ref.[64] Linear fits for the non-methoxy-substituted PAs in (a) and (b) result in a slope of –0.32 ± 0.04 eV/D and –0.53 ± 0.05 eV/D, respectively. The slope –0.53 eV/D (in CGS units) corresponds to $-2.5 \cdot 10^{10}$ V/m (in SI units).

In **Table 3** we compare our results with three examples from literature. These examples should be comparable with the present system because in each case the substrate is a metal oxide (polycrystalline or amorphous) and phosphonic acids are used to modify Φ. The two parameters listed in Table 3 are the observed range in $\Delta\Phi_{SAM}$ and the slope obtained from a linear fit of Φ versus μ_z. The range in $\Delta\Phi_{SAM}$ observed here for AlO_x/Al (0.91 eV) is slightly smaller than the range reported for ITO (1.2 eV) and GZO (1.09 eV). This range can obviously be widened through structural modifications that allow the phosphonic acid molecules to pack more densely or that increase their dipole moment. The second parameter in Table 3, the slope of Φ versus μ_z, is predicted by Eq. 4 to be equal to $e \cdot N / (\varepsilon_0 \cdot \varepsilon_{SAM})$. Using the experimental molecular density N from the dense reference monolayer, SAM **1** (4.15 nm^{-2}; Table 2), and an estimation for the dielectric constant of the SAM ($\varepsilon_{SAM} \approx 2.5$)[16,48,67-69], the predicted slope is $3.0 \cdot 10^{10}$ V/m in SI units (0.62 eV/D in CGS units), which is very close to the value determined experimentally based on photoemission data and DFT calculations ($-2.5 \cdot 10^{10}$ V/m, see Figure 5b). Thus our data shows that for fluorinated benzylphosphonic acids on AlO_x/Al, the dependence of work function on molecular dipole moment is in excellent agreement with the prediction from the Helmholtz model. To our knowledge, the present study for the first time demonstrates that PAs on AlO_x/Al substrates exhibit a linear correlation between the molecular dipole moments and the measured work function, and that this correlation is consistent with Eq. 4, although an earlier report by Nüesch et al.[70] provide indications that SAMs of dipolar benzoic acid derivatives might follow a similar trend. We are aware of the fact that the Helmholtz equation is just a simple approximation and that a full DFT calculation, accounting for the polarisation from the environment, provides a more accurate picture of the electron density distribution in a 2-dimensional monolayer.[71] However, such calculations are computationally very expensive and require a careful theoretic treatment, and it turns out that the

present simpler (semi-empirical) approach is well suited for a fast verification of experimental work function data.

Table 3. Dependence of experimental work function values on the dipole moment: comparison with literature results. The last column on the right side represents the approximate density according to the reported references.

Source	Substrate	Range of $\Delta\Phi_{SAM}$ (eV)	Slope of Φ *vs.* μ_z (eV/D)	N (nm^{-2})
this work	AlO_x/Al	0.9_1	-0.53[a]	2.3–5.6[b]
Ref.[37]	ITO[c]	1.2	-0.47[d]	~0.75[l]
Ref.[44]	GZO[c]	1.1_9	-0.27[e]	~1.4
Ref.[36]	ZnO[f]	1.5	0.30[g]	~2
Ref.[46]	ZnO[h]	2.3	0.43[i]	~2

[a]Slope obtained with normalized work functions (Φ_{norm}; see text). [b]Observed range (average N = 3.6 nm^{-2}. [c]Polycrystalline film. [d]Value estimated from Figure 5 of Ref.[37] [e]Value estimated from Figure 6 of Ref.[44] [f]Single crystal. [g]Value reported in Figure 2 of Ref.[36] [h]Sol-gel film. [i]Value estimated from Figure 2 of Ref.[46] [l]Value taken from Ref.[72]

Discussion

We have focused in this paper on using PAs to modify two important properties of AlO_x/Al electrodes: surface energy (γ_S, Figure 3) and work function (Φ, Figure 5). The adhesion between electrode and organic layer is often a limiting factor in device stability and it may also affect the charge injection barrier. Thus, the ability to tune γ_S, and thereby varying the adhesion, can be critical to optimize device performance. The deposition of a SAM as an interlayer between the electrode and the organic layer is a simple and reproducible way to modify γ_S. Although several classes of compounds are known to form SAMs on AlO_x/Al and other metal oxides, notably carboxylic acids and silanes, phosphonic acids generally appear to be superior for this purpose. We included dodecylphosphonic acid (**1**) in this study as an example of an alkyl phosphonic acid. Although the SAM of **1** is formed reproducibly, its surface energy (23.5 mJ/m^2) may be too low for an efficient adhesion of organic semiconductors, which intrinsically contain polarizable aromatic groups. On the other hand, γ_S for SAM **12** (70.5 mJ/m^2) is nearly as polar as the SC/UVO-cleaned AlO_x/Al (76.5

mJ/m^2) and may be too high for good adhesion of those organic semiconductors containing aliphatic groups. The remaining PAs (**2** to **11**) make it possible to vary γ_S smoothly from 56.2 to 31.5 mJ/m^2, with an average increment of ~3 mJ/m^2 (Table 1).

The SAMs presented in this study display a relatively wide distribution of molecular densities (*N*), with values ranging from 2.3 to 5.6 molecules per nm^2 (Table 2). The variety of intermolecular interactions possible within these SAMs, from steric to electrostatic (depending on the specific fluorine substitution pattern and presence or absence of methoxy substituent), may account for this range of densities, but the amorphous nature of the AlO_x layer (including roughness and inhomogeneity) should also be considered. As noted in the experimental section, these considerations led us to select the SC/UVO instead of the SC/OP pretreatment as a means of providing possibly reproducible substrates for SAM formation. However, other factors besides substrate pretreatment can affect SAM quality, in particular the solvent, the concentration in the assembly solution, and the assembly time. We chose to keep these conditions constant (within reasonable bounds) for all SAMs, while recognizing that some of the PAs derivatives were more soluble in absolute ethanol than others. Of course, this can affect SAM density as well as sample reproducibility. Based on our results, we estimate the reproducibility in SAM density (coverage) to be 15% or better for PAs **1**, **4**, **5**, **6**, **8**, **9**, **10**, **11**, and **12**, and 30% or better for the remaining PAs (**2**, **3**, and **7**).

The Helmholtz equation (Eq. 4) predicts that the SAM-induced shift in the surface potential is proportional to molecular density (*N*). To compensate for the variation in *N* within the SAMs, we have normalized Φ with respect to *N*, using the dodecyl phosphonic SAM (**1**) as reference (Eq. 5). The resulting plot of Φ_{norm} versus $\mu_z - \mu_z^{ref}$ displays the predicted linear relationship (Figure 5b). Without this normalization, the plot of Φ versus $\mu_z - \mu_z^{ref}$ shows the same trend, however the correlation is poorer and the slope is too small (Figure 5a). Including normalization, the experimental slope is close to that predicted by the Helmholtz equation, meaning that the molecular orientation derived from the DFT cluster model is realistic, and that the depolarization effect must be minor. Furthermore, the contribution from the bond dipole is already included in the DFT

calculation, so it will not much affect the results, besides that it is approximately constant for all phosphonic acids investigated here (i.e., it has little impact on the slope in Figure 5). Interestingly, the linear trend for the methoxy-terminated SAMs is offset from that for H- or F-terminated SAMs, while the slopes are practically the same.

Notwithstanding the spread in packing densities, we could demonstrate that the present set of compounds allows modification of the work function of AlO_x/Al surfaces over a wide range from 3.18 eV to 4.09 eV ($\Delta\Phi$ = 0.91 eV). Despite the very low work function obtained with **1**, this compound might be undesirable from a device perspective as an extremely hydrophobic surface is created. Thus, the *ortho* disubstituted benzylic phosphonic acid derivative **6** might be a valid alternative to realize low work function electrodes, whenever a more polar component of the surface energy is required. For compound **6**, the fluorine substituents close to the benzylic functionality direct the negative charge towards the surface, thus creating the most positive dipole moment and thus the lowest work function within the series (Figure 5b). On the other end of the scale, derivative **9** shows a work function suited, e.g., for hole injection into *p*-type semiconducting materials (in particular if a SAM having a higher molecular density could be realized). All the other derivatives provide intermediate work function values in the range of 3.4–4.2 eV, and might offer a handle to tune the energy alignment between Fermi level and semiconductor transport level, for example for electron injection at cathode-acceptor interfaces. We should mention that one can separate the surface energy contribution from the work function modulation by introducing dipoles embedded in the molecular structure, such that the adhesion of the semiconductor to the electrode is kept constant.[73] This approach may require a significant synthetic effort, but such effort could be justified in cases where the work function needs to be adjusted for an organic semiconductor of special interest or technical relevance.

The structural and chemical properties of fluorinated phosphonic acid monolayers on AlO_x/Al surfaces, which have not been touched upon in this paper, are disclosed in a dedicated XPS and infrared (PM-IRRAS) follow-up study.[29]

Conclusions

Through the synthesis of five previously unreported fluorinated benzylphosphonic acids, and by the systematic study of the self-assembled monolayers from these and other commercially available PA derivatives, a broad range of surface free energy (γ_S) and work function (Φ) values has been demonstrated on AlO_x/Al surfaces. Whereas previous investigations have proven the utility of this class of PAs for modifying the surface properties of a variety of metal oxides, the present study provides a first quantitative assessment on the correlation between the work function of AlO_x/Al substrates and the molecular dipole moment of the chemisorbed molecular adsorbates. We have employed a novel approach to make this correlation, namely by combining XPS data to determine the molecular density (N) with DFT results from Al_6O_{10}-based cluster models to compute μ_z. Using this data, we make use of a simple procedure to normalize Φ with respect to the molecular density. Our results show a remarkably good agreement of the experimental work function values with the Helmholtz model (Eq. 4). This correlation is especially surprising when considering the amorphous character of the AlO_x/Al surface. Overall, contact angle and XPS data demonstrate that these PA derivatives form dense and reproducible monolayers on AlO_x/Al, despite the characteristic roughness of alumina substrates. The present study will help researchers to engineer the surface properties of one of today's most relevant electrode materials, both in terms of adhesion (stability) and energy level alignment at metal-semiconductor interfaces (injection, blocking), for immediate applications in devices such as OLEDs, OTFTs, organic solar cells, and printed organic circuits.

Acknowledgement: The authors acknowledge Carsten Menke (Biovia) for valuable support in Dmol^3 issues.

Supporting Information Available. Synthesis procedures and NMR spectra of novel phosphonic acid derivatives, molecular modeling results, LI-XPS results, and a derivation of Eq. 5 are available free of charge via the Internet at http://pubs.acs.org.

TOC figure:

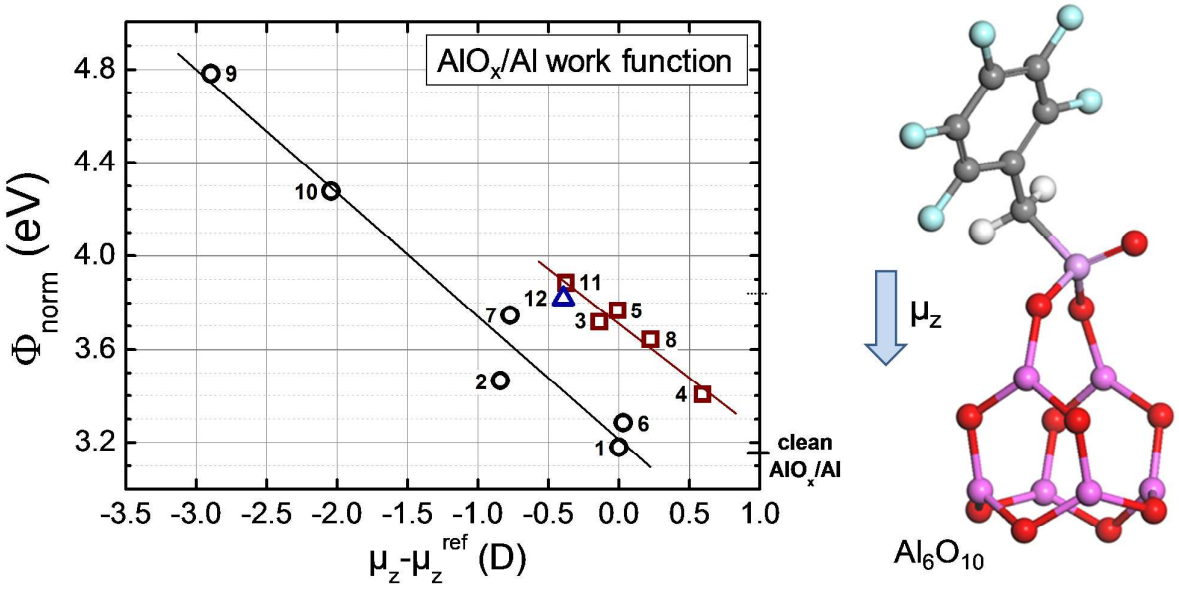

Reference List

(1) Mann, B.; Kuhn, H. Tunneling through Fatty Acid Salt Monolayers. *J. Appl. Phys.* **1971,** *42*, 4398-4405.

(2) Love, J. C.; Estroff, L. A.; Kriebel, J. K.; Nuzzo, R. G.; Whitesides, G. M. Self-Assembled Monolayers of Thiolates on Metals as a Form of Nanotechnology. *Chem. Rev.* **2005,** *105*, 1103-1169.

(3) Mathijssen, S. G. J.; van Hal, P. A.; van den Biggelaar, T. J. M.; Smits, E. C. P.; de Boer, B.; Kemerink, M.; Janssen, R. A. J.; de Leeuw, D. M. Manipulating the Local Light Emission in Organic Light-Emitting Diodes by using Patterned Self-Assembled Monolayers. *Adv. Mater.* **2008,** *20*, 2703-2706.

(4) Sirringhaus, H. Device Physics of Solution-Processed Organic Field-Effect Transistors. *Adv. Mater.* **2005,** *17*, 2411-2425.

(5) Campbell, I. H.; Rubin, S.; Zawodzinski, T. A.; Kress, J. D.; Martin, R. L.; Smith, D. L.; Barashkov, N. N.; Ferraris, J. P. Controlling Schottky Energy Barriers in Organic Electronic Devices Using Self-Assembled Monolayers. *Phys. Rev. B* **1996,** *54*, 14321-14324.

(6) Heimel, G.; Romaner, L.; Zojer, E.; Brédas, J.-L. The Interface Energetics of Self-Assembled Monolayers on Metals. *Acc. Chem. Res.* **2008,** *41*, 721-729.

(7) Campbell, I. H.; Kress, J. D.; Martin, R. L.; Smith, D. L.; Barashkov, N. N.; Ferraris, J. P. Controlling Charge Injection in Organic Electronic Devices Using Self-Assembled Monolayers. *Appl. Phys. Lett.* **1997,** *71*, 3528-3530.

(8) de Boer, B.; Hadipour, A.; Mandoc, M. M.; van Woudenbergh, T.; Blom, P. W. M. Tuning of Metal Work Functions with Self-Assembled Monolayers. *Adv. Mater.* **2005,** *17*, 621-625.

(9) Ford, W. E.; Gao, D.; Knorr, N.; Wirtz, R.; Scholz, F.; Karipidou, Z.; Ogasawara, K.; Rosselli, S.; Rodin, V.; Nelles, G.; von Wrochem, F. Organic Dipole Layers for Ultralow Work Function Electrodes. *ACS Nano* **2014,** *8*, 9173-9180.

(10) Ulman, A. Formation and Structure of Self-Assembled Monolayers. *Chem. Rev.* **1996,** *96*, 1533-1554.

(11) Lee, J.; Jung, B. J.; Lee, J. I.; Chu, H. Y.; Do, L. M.; Shim, H. K. Modification of an ITO Anode with a Hole-Transporting SAM for Improved OLED Device Characteristics. *J. Mater. Chem.* **2002,** *12*, 3494-3498.

(12) Turak, A. Interfacial Degradation in Organic Optoelectronics. *RSC Adv.* **2013,** *3*, 6188-6225.

(13) Laibinis, P. E.; Whitesides, G. M. omega-Terminated Alkanethiolate Monolayers on Surfaces of Copper, Silver, and Gold have Similar Wettabilities. *J. Am. Chem. Soc.* **1992,** *114*, 1990-1995.

(14) Halik, M.; Klauk, H.; Zschieschang, U.; Schmid, G.; Dehm, C.; Schuetz, M.; Effenberger, F.; Brunnbauer, M.; Stellacci, F. Low-voltage Organic Transistors with an Amorphous Molecular Gate Dielectric. *Nature* **2004,** *431*, 963-966.

(15) Klauk, H.; Zschieschang, U.; Pflaum, J.; Halik, M. Ultralow-Power Organic Complementary Circuits. *Nature* **2007,** *445*, 745-748.

(16) Salinas, M.; Jäger, C. M.; Amin, A. Y.; Dral, P. O.; Meyer-Friedrichsen, T.; Hirsch, A.; Clark, T.; Halik, M. The Relationship between Threshold Voltage and Dipolar Character of Self-Assembled Monolayers in Organic Thin-Film Transistors. *J. Am. Chem. Soc.* **2012,** *134*, 12648-12652.

(17) Gawalt, E. S.; Avaltroni, M. J.; Danahy, M. P.; Silverman, B. M.; Hanson, E. L.; Midwood, K. S.; Schwarzbauer, J. E.; Schwartz, J. Bonding Organics to Ti Alloys: Facilitating Human Osteoblast Attachment and Spreading on Surgical Implant Materials. *Langmuir* **2002,** *19*, 200-204.

(18) Quinones, R.; Gawalt, E. S. Polystyrene Formation on Monolayer-Modified Nitinol Effectively Controls Corrosion. *Langmuir* **2008,** *24*, 10858-10864.

(19) Barr, T. L. An ESCA Study of the Termination of the Passivation of Elemental Metals. *J. Phys. Chem.* **1978,** *82*, 1801-1810.

(20) Popova, I.; Zhukov, V.; Yates, J. T. Depth-Dependent Electrical Impedance Distribution in Al2O3 Films on Al(111)Detection of an Inner Barrier Layer. *Langmuir* **2000,** *16*, 10309-10314.

(21) Quade, A.; Wulff, H.; Steffen, H.; Tun, T. M.; Hippler, R. Investigation of the Aluminium Oxidation in an Oxygen Plasma Excited by Microwaves. *Thin Solid Films* **2000,** *377–378*, 626-630.

(22) Giza, M.; Thissen, P.; Grundmeier, G. Adsorption Kinetics of Organophosphonic Acids on Plasma-Modified Oxide-Covered Aluminum Surfaces. *Langmuir* **2008,** *24*, 8688-8694.

(23) Strohmeier, B. R. An ESCA Method for Determining the Oxide Thickness on Aluminum Alloys. *Surf. Interface Anal.* **1990,** *15*, 51-56.

(24) Owens, D. K.; Wendt, R. C. Estimation of the Surface Free Energy of Polymers. *J. Appl. Polym. Sci.* **1969,** *13*, 1741-1747.

(25) *NIST X-ray Photoelectron Spectroscopy Database 20 - Version 4.1;* 2012.

(26) Koch, N.; Kahn, A.; Ghijsen, J.; Pireaux, J.-J.; Schwartz, J.; Johnson, R. L.; Elschner, A. Conjugated Organic Molecules on Metal versus Polymer Electrodes: Demonstration of a Key Energy Level Alignment Mechanism. *Appl. Phys. Lett.* **2003,** *82*, 70-72.

(27) Perdew, J. P.; Burke, K.; Ernzerhof, M. Generalized Gradient Approximation Made Simple. *Phys. Rev. Lett.* **1996,** *77*, 3865-3868.

(28) Delley, B. An All-Electron Numerical Method for Solving the Local Density Functional for Polyatomic Molecules. *J. Chem. Phys.* **1990,** *92*, 508-517.

(29) Ford, W. E.; Abraham, F.; Scholz, F.; Nelles, G.; Sandford, G.; von Wrochem, F. Spectroscopic Characterization of Fluorinated Benzylphosphonic Acid Monolayers on AlO_x/Al Surfaces. *Submitted* **2016**.

(30) Casarin, M.; Maccato, C.; Vittadini, A. Theoretical Study of the Chemisorption of CO on Al2O3(0001). *Inorg. Chem.* **2000,** *39*, 5232-5237.

(31) Gianotto, A. K.; Rawlinson, J. W.; Cossel, K. C.; Olson, J. E.; Appelhans, A. D.; Groenewold, G. S. Hydration of Alumina Cluster Anions in the Gas Phase. *J. Am. Chem. Soc.* **2004,** *126*, 8275-8283.

(32) Sierka, M.; Döbler, J.; Sauer, J.; Santambrogio, G.; Brümmer, M.; Wöste, L.; Janssens, E.; Meijer, G.; Asmis, K. Unexpected Structures of Aluminum Oxide Clusters in the Gas Phase. *Angew. Chem. Int. Ed.* **2007,** *46*, 3372-3375.

(33) Bermudez, V. M. Quantum-Chemical Study of the Adsorption of DMMP and Sarin on γ–Al2O3. *J. Phys. Chem. C* **2007,** *111*, 3719-3728.

(34) Alexander, M. R.; Thompson, G. E.; Beamson, G. Characterization of the Oxide/Hydroxide Surface of Aluminium Using X-Ray Photoelectron Spectroscopy: a Procedure for Curve Fitting the O 1s Core Level. *Surf. Interface Anal.* **2000,** *29*, 468-477.

(35) Thissen, P.; Valtiner, M.; Grundmeier, G. Stability of Phosphonic Acid Self-Assembled Monolayers on Amorphous and Single-Crystalline Aluminum Oxide Surfaces in Aqueous Solution. *Langmuir* **2010,** *26*, 156-164.

(36) Lange, I.; Reiter, S.; Pätzel, M.; Zykov, A.; Nefedov, A.; Hildebrandt, J.; Hecht, S.; Kowarik, S.; Wöll, C.; Heimel, G.; Neher, D. Tuning the Work Function of Polar Zinc Oxide Surfaces using Modified Phosphonic Acid Self-Assembled Monolayers. *Adv. Funct. Mater.* **2014,** *24*, 7014-7024.

(37) Hotchkiss, P. J.; Li, H.; Paramonov, P. B.; Paniagua, S. A.; Jones, S. C.; Armstrong, N. R.; Bredas, J. L.; Marder, S. R. Modification of the Surface Properties of Indium Tin Oxide with Benzylphosphonic Acids: A Joint Experimental and Theoretical Study. *Adv. Mater.* **2009,** *21*, 4496-4501.

(38) Knesting, K. M.; Hotchkiss, P. J.; MacLeod, B. A.; Marder, S. R.; Ginger, D. S. Spatially Modulating Interfacial Properties of Transparent Conductive Oxides: Patterning Work Function with Phosphonic Acid Self-Assembled Monolayers. *Adv. Mater.* **2012,** *24*, 642-646.

(39) Wood, C.; Li, H.; Winget, P.; Brédas, J. L. Binding Modes of Fluorinated Benzylphosphonic Acids on the Polar ZnO Surface and Impact on Work Function. *J. Phys. Chem. C* **2012,** *116*, 19125-19133.

(40) MacLeod, B. A.; Horwitz, N. E.; Ratcliff, E. L.; Jenkins, J. L.; Armstrong, N. R.; Giordano, A. J.; Hotchkiss, P. J.; Marder, S. R.; Campbell, C. T.; Ginger, D. S. Built-In Potential in Conjugated Polymer Diodes with Changing Anode Work Function: Interfacial States and Deviation from the Schottky–Mott Limit. *J. Phys. Chem. Lett.* **2012,** *3*, 1202-1207.

(41) Ndione, P. F.; Garcia, A.; Widjonarko, N. E.; Sigdel, A. K.; Steirer, K. X.; Olson, D. C.; Parilla, P. A.; Ginley, D. S.; Armstong, N. R.; Richards, R. E.; Ratcliff, E. L.; Berry, J. J. Highly-Tunable Nickel Cobalt Oxide as a Low-Temperature P-Type Contact in Organic Photovoltaic Devices. *Adv. Energy Mater.* **2013,** *3*, 524-531.

(42) Bulusu, A.; Paniagua, S. A.; MacLeod, B. A.; Sigdel, A. K.; Berry, J. J.; Olson, D. C.; Marder, S. R.; Graham, S. Efficient Modification of Metal Oxide Surfaces with Phosphonic Acids by Spray Coating. *Langmuir* **2013,** *29*, 3935-3942.

(43) Knesting, K. M.; Ju, H.; Schlenker, C. W.; Giordano, A. J.; Garcia, A.; Smith, O. N. L.; Olson, D. C.; Marder, S. R.; Ginger, D. S. ITO Interface Modifiers Can Improve VOC in Polymer Solar Cells and Suppress Surface Recombination. *J. Phys. Chem. Lett.* **2013,** *4*, 4038-4044.

(44) Li, H.; Ratcliff, E. L.; Sigdel, A. K.; Giordano, A. J.; Marder, S. R.; Berry, J. J.; Brédas, J. L. Modification of the Gallium-Doped Zinc Oxide Surface with Self-Assembled Monolayers of Phosphonic Acids: A Joint Theoretical and Experimental Study. *Adv. Funct. Mater.* **2014,** *24*, 3593-3603.

(45) Shao, G.; Glaz, M. S.; Ma, F.; Ju, H.; Ginger, D. S. Intensity-Modulated Scanning Kelvin Probe Microscopy for Probing Recombination in Organic Photovoltaics. *ACS Nano* **2014,** *8*, 10799-10807.

(46) Lange, I.; Reiter, S.; Kniepert, J.; Piersimoni, F.; Pätzel, M.; Hildebrandt, J.; Brenner, T.; Hecht, S.; Neher, D. Zinc Oxide Modified with Benzylphosphonic Acids as Transparent Electrodes in Regular and Inverted Organic Solar Cell Structures. *Appl. Phys. Lett.* **2015,** *106*, 113302.

(47) Sang, L.; Mudalige, A.; Sigdel, A. K.; Giordano, A. J.; Marder, S. R.; Berry, J. J.; Pemberton, J. E. PM-IRRAS Determination of Molecular Orientation of Phosphonic Acid Self-Assembled Monolayers on Indium Zinc Oxide. *Langmuir* **2015,** *31*, 5603-5613.

(48) Paniagua, S. A.; Hotchkiss, P. J.; Jones, S. C.; Marder, S. R.; Mudalige, A.; Marrikar, F. S.; Pemberton, J. E.; Armstrong, N. R. Phosphonic Acid Modification of Indium − Tin Oxide Electrodes: Combined XPS/UPS/Contact Angle Studies. *J. Phys. Chem. C* **2008,** *112*, 7809-7817.

(49) Liakos, I. L.; Newman, R. C.; McAlpine, E.; Alexander, M. R. Comparative Study of Self-Assembly of a Range of Monofunctional Aliphatic Molecules on Magnetron-Sputtered Aluminium. *Surf. Interface Anal.* **2004,** *36*, 347-354.

(50) Silverman, B. M.; Wieghaus, K. A.; Schwartz, J. Comparative Properties of Siloxane vs Phosphonate Monolayers on A Key Titanium Alloy. *Langmuir* **2004,** *21*, 225-228.

(51) Hotchkiss, P. J.; Jones, S. C.; Paniagua, S. A.; Sharma, A.; Kippelen, B.; Armstrong, N. R.; Marder, S. R. The Modification of Indium Tin Oxide with Phosphonic Acids: Mechanism of Binding, Tuning of Surface Properties, and Potential for Use in Organic Electronic Applications. *Acc. Chem. Res.* **2011,** *45*, 337-346.

(52) Bhairamadgi, N. S.; Pujari, S. P.; Trovela, F. G.; Debrassi, A.; Khamis, A. A.; Alonso, J. M.; Al Zahrani, A. A.; Wennekes, T.; Al Turaif, H. A.; van Rijn, C.; Alhamed, Y. A.; Zuilhof, H. Hydrolytic and Thermal Stability of Organic Monolayers on Various Inorganic Substrates. *Langmuir* **2014,** *30*, 5829-5839.

(53) Thissen, P.; Vega, A.; Peixoto, T.; Chabal, Y. J. Controlled, Low-Coverage Metal Oxide Activation of Silicon for Organic Functionalization: Unraveling the Phosphonate Bond. *Langmuir* **2012,** *28*, 17494-17505.

(54) Adamson, A. W.; Gast, A. P. *Physical Chemistry of Surfaces;* Sixth Edition ed.; Wiley-Interscience: New York, 1997.

(55) O'Hagan, D. Understanding Organofluorine Chemistry. An Introduction to the C-F Bond. *Chem. Soc. Rev.* **2008,** *37*, 308-319.

(56) Gliboff, M.; Li, H.; Knesting, K. M.; Giordano, A. J.; Nordlund, D.; Seidler, G. T.; Brédas, J. L.; Marder, S. R.; Ginger, D. S. Competing Effects of Fluorination on the Orientation of Aromatic and Aliphatic Phosphonic Acid Monolayers on Indium Tin Oxide. *J. Phys. Chem. C* **2013,** *117*, 15139-15147.

(57) Lindberg, B. J.; Johansson, G.; Gelius, U.; Fahlman, A.; Nordling, C.; Siegbahn, K. Molecular Spectroscopy by Means of ESCA. *Physica Scripta* **1970,** *1*, 286-298.

(58) Duwez, A.-S. Exploiting Electron Spectroscopies to Probe the Structure and Organization of Self-Assembled Monolayers: a Review. *J. El. Spec. Rel. Phenom.* **2004,** *134*, 97-138.

(59) Zharnikov, M. High-Resolution X-Ray Photoelectron Spectroscopy in Studies of Self-Assembled Organic Monolayers. *J. El. Spec. Rel. Phenom.* **2010,** *178*, 380-393.

(60) Schreiber, F. Structure and Growth of Self-Assembling Monolayers. *Prog. Surf. Sci.* **2000,** *65*, 151-256.

(61) Gao, W.; Dickinson, L.; Grozinger, C.; Morin, F. G.; Reven, L. Order–Disorder Transitions in Self-Assembled Monolayers: A ^{13}C Solid-State NMR Study. *Langmuir* **1997,** *13*, 115-118.

(62) Pawsey, S.; Yach, K.; Reven, L. Self-Assembly of Carboxyalkylphosphonic Acids on Metal Oxide Powders. *Langmuir* **2002,** *18*, 5205-5212.

(63) von Wrochem, F.; Gao, D.; Scholz, F.; Nothofer, H. G.; Nelles, G.; Wessels, J. M. Efficient Electronic Coupling and Improved Stability with Dithiocarbamate-Based Molecular Junctions. *Nature Nanotech.* **2010,** *5*, 618-624.

(64) Wang, W. F.; Alsmeier, J. H.; Wolak, M.; Schlaf, R. Determination of the Charge Neutrality Level of Poly(3-hexylthiophene). *J. Chem. Phys.* **2013,** *138*, 054705.

(65) Braun, S.; Salaneck, W. R.; Fahlman, M. Energy-Level Alignment at Organic/Metal and Organic/Organic Interfaces. *Adv. Mater.* **2009,** *21*, 1450-1472.

(66) Paramonov, P. B.; Paniagua, S. A.; Hotchkiss, P. J.; Jones, S. C.; Armstrong, N. R.; Marder, S. R.; Bredas, J. L. Theoretical Characterization of the Indium Tin Oxide Surface and of Its Binding Sites for Adsorption of Phosphonic Acid Monolayers. *Chem. Mater.* **2008,** *20*, 5131-5133.

(67) Demoz, A.; Harrison, D. J. Characterization and Extremely Low Defect Density Hexadecanethiol Monolayers on Mercury Surfaces. *Langmuir* **1993,** *9*, 1046-1050.

(68) Rampi, M. A.; Schueller, O. J. A.; Whitesides, G. M. Alkanethiol Self-Assembled Monolayers as the Dielectric of Capacitors with Nanoscale Thickness. *Appl. Phys. Lett.* **1998,** *72*, 1781-1783.

(69) Porter, M. D.; Bright, T. B.; Allara, D. L.; Chidsey, C. E. D. Spontaneously Organized Molecular Assemblies. 4. Structural Characterization of n-Alkyl Thiol Monolayers on Gold by Optical Ellipsometry, Infrared Spectroscopy, and Electrochemistry. *J. Am. Chem. Soc.* **1987,** *109*, 3559-3568.

(70) Nüesch, F.; Carrara, M.; Zuppiroli, L. Solution versus Vapor Growth of Dipolar Layers on Activated Oxide Substrates. *Langmuir* **2003,** *19*, 4871-4875.

(71) Heimel, G.; Romaner, L.; Zojer, E.; Brédas, J. L. Toward Control of the Metal/Organic Interfacial Electronic Structure in Molecular Electronics: A First-Principles Study on Self-Assembled Monolayers of π-conjugated Molecules on Noble Metals. *Nano Lett.* **2007,** *7*, 932-940.

(72) Koh, S. E.; McDonald, K. D.; Holt, D. H.; Dulcey, C. S.; Chaney, J. A.; Pehrsson, P. E. Phenylphosphonic Acid Functionalization of Indium Tin Oxide: Surface Chemistry and Work Functions. *Langmuir* **2006,** *22*, 6249-6255.

(73) bu-Husein, T.; Schuster, S.; Egger, D. A.; Kind, M.; Santowski, T.; Wiesner, A.; Chiechi, R.; Zojer, E.; Terfort, A.; Zharnikov, M. The Effects of Embedded Dipoles in Aromatic Self-Assembled Monolayers. *Adv. Func. Mat.* **2015,** *25*, 3943-3957.